



A space–time finite element method for structural acoustics in infinite domains

Part 2: Exact time-dependent non-reflecting boundary conditions

Lonny L. Thompson^{*}, Peter M. Pinsky¹

Department of Civil Engineering, Stanford University, Stanford, CA 94305-4020, USA

Received 24 August 1994; revised 14 September 1995

Abstract

In Part 1, a new space–time finite element method for transient structural acoustics in exterior domains was given. The formulation employs a finite computational fluid domain surrounding the structure and incorporates local time-dependent non-reflecting boundary conditions on the fluid truncation boundary. In this paper, new exact time-dependent non-reflecting boundary conditions are developed for solutions of the scalar wave equation in three space dimensions. These high-order accurate absorbing boundary conditions are based on the exact impedance relation for the acoustic fluid through the Dirichlet-to-Neumann (DtN) map in the frequency domain and are exact for solutions consisting of the first N spherical wave harmonics. Time-dependent boundary conditions are obtained through an inverse Fourier transform procedure. Two alternative sequences of boundary conditions are derived: the first involves both temporal and spatial derivatives (local in time and local in space version), and the second involves temporal derivatives and a spatial integral (local in time and non-local in space version). These non-reflecting boundary conditions are incorporated as ‘natural’ boundary conditions in the space–time variational equation, i.e. they are enforced weakly in both space and time. Several numerical examples involving transient radiation are presented to illustrate the high-order accuracy and efficiency achieved by the new space–time finite element formulation for transient structural acoustics with non-reflecting boundaries.

1. Introduction

When domain-based computational methods such as the space–time finite element method are used to model the coupled structural acoustics problem in infinite domains, accurate non-reflecting boundary conditions are required on an artificial truncation boundary Γ_x that surrounds the structure. If the form of the non-reflecting boundary condition is over-simplified, spurious reflected waves can be generated at the artificial boundary, which can substantially degrade the accuracy of the numerical solution. For example, the simple ‘plane-wave’ (PW)-damper defined in [1]:

$$\frac{\partial \phi}{\partial n}(\mathbf{x}, t) = -\mathcal{S}_0 \phi(\mathbf{x}, t), \quad \mathbf{x} \in \Gamma_x, t > 0 \quad (1)$$

^{*} Corresponding author. Assistant Professor of Mechanical Engineering and Engineering Mechanics, Clemson University, Clemson, SC 29634-0921, USA.

¹ Associate Professor.

with the local differential operator

$$\mathbb{S}_0 := \frac{1}{c} \frac{\partial}{\partial t}$$

where $\partial\phi/\partial n$ is the normal derivative to Γ_x , ϕ is the solution variable for the second-order hyperbolic wave equation, and c is the wave speed for the acoustic medium; while exact in one dimension, deteriorates significantly in multi-dimensions as the position of the truncation boundary approaches the source of radiation, especially in the low-frequency (long wavelength) limit. In order to minimize the effect of spurious reflections, the computational region can be enlarged so that the artificial boundary is far from the radiator/scatterer, however, this will require an increase in the number of solution variables, with a subsequent increase in the matrix size and computational expense. It is thus preferable to use on the truncation boundary Γ_x , a non-reflecting boundary condition that is sufficiently accurate even when Γ_x is positioned near the radiating structure.

For time-harmonic steady-state analysis it is possible to obtain an exact non-reflecting boundary condition on a separable truncation boundary through the Dirichlet-to-Neumann (DtN) map [2], in the frequency domain. The DtN map is a non-local (integral) operator composed of a series of wave harmonics relating Dirichlet-to-Neumann data on the artificial boundary. Although the DtN map is a non-local operator coupling all points on the artificial boundary, it is easily implemented in the finite element method as a ‘natural’ boundary condition using standard C^0 continuous interpolation functions in the frequency domain. The advantage of the non-local DtN boundary condition over local (differential) boundary conditions based on high-frequency or power series approximations, is that high-order accuracy can be achieved simply by taking more terms in the DtN series, without having to compute high-order differential operators. In addition, the physical interpretation of the DtN map as an exact representation of the exterior acoustic impedance restricted to Γ_x in terms of wave harmonics assures the stability of the solution and validity of the non-reflecting boundary condition over the entire frequency spectrum.

Motivated by the good stability and accuracy properties of the DtN map in the frequency domain, it is natural to attempt to extend these ideas to the time-domain. A direct time-dependent counterpart to the DtN map can be obtained through a convolution integral in time, resulting in a boundary condition that is non-local in both space and time dimensions. Unfortunately, while this condition is stable and exact for solutions consisting of the first N wave harmonics by design, the implementation requires storage of all previous solutions up to the current time step, and is not feasible for large-scale computations over long time intervals.

Because of the limitations and difficulties associated with the time convoluted DtN map, we were motivated to find a time-dependent counterpart to the DtN map which retains the property of being exact for the first N wave harmonics on the truncation boundary, while replacing the temporal convolution integral with local temporal derivatives. In this way the boundary conditions at time t will involve only the values of the solution and its derivatives at time t , and not values at previous times, resulting in an efficient yet accurate solution. In this paper, two new sequences of time-dependent non-reflecting boundary operators are derived starting from the DtN map in the frequency domain; the first involves both time and spatial derivatives (local in time and local in space version), and the second involves time derivatives yet retains a spatial integral (local in time and non-local in space version). Another boundary condition for time-dependent acoustic problems that is also based on the DtN method has been proposed in [3].

The development of our local in time and local in space boundary conditions begins with the exact localization of the non-local DtN map in the frequency domain [4, 5]. After recognizing a special property of the impedance coefficients of the local DtN map, time-dependent boundary conditions are then obtained through direct application of an inverse Fourier transform. Since these new time-dependent boundary conditions follow directly from the exact impedance expressed through the DtN map, they are exact in both time and space for solutions consisting of the first N wave harmonics on the artificial boundary.

As the order of these local non-reflecting boundary conditions increases, they become increasingly difficult to implement in standard semidiscrete finite element formulations due to the occurrence of

high-order time derivatives on the fluid truncation boundary. In this paper we demonstrate that the time-discontinuous Galerkin Least-Squares space-time finite element formulation developed in [6–8], provides a natural variational setting for the incorporation of these local in time boundary conditions. Crucial to the stability and convergence of the method is the introduction of consistent temporal jump operators across space-time slabs restricted to the artificial boundary. The specific form of these operators is designed such that continuity of the solution across slabs is weakly enforced in a form consistent with the non-reflecting boundary conditions. However, for boundary conditions extending beyond second-order, high-order continuity in the space dimension on Γ_x is required due to the appearance of high-order tangential derivatives. To address this issue we show that a local in time inverse Fourier transform exists for the non-local in space and frequency dependent Dirichlet-to-Neumann (DtN) map [2], allowing for boundary conditions that are non-local in space while retaining the important property of locality in time. This new sequence has the advantage that when implemented in the time-discontinuous finite element formulation, standard C^0 interpolation functions may be used for both the space and time dimensions.

As a result of starting from the exact DtN map in the frequency domain, the time-dependent non-reflecting boundary conditions proposed in this paper exactly represent the transient solution as a series of outgoing wave harmonics. This property plays an important role in the understanding of how individual wave harmonics contribute to the accuracy and stability of the solution as effected by the radial distance of the artificial boundary from the source, the geometric complexity of the wave pattern and the frequency content of the transient waves. In contrast, a physical understanding of the harmonic contribution to the accuracy and stability of absorbing boundary conditions based on high-frequency approximations, such as the sequence derived by Engquist and Majda [9, 10], or boundary operators based on radial power series (multipole) expansions, such as the popular sequence derived by Bayliss and Turkel [11, 12], is currently lacking.

2. Dirichlet-to-Neumann map in the frequency domain

In order to obtain a sequence of time-dependent non-reflecting boundary conditions which are exact for the first N spherical wave harmonics on the truncation boundary Γ_x , we start with the Dirichlet-to-Neumann (DtN) map in the frequency domain. The DtN map represents the exact impedance for the infinite acoustic fluid restricted to an artificial boundary of separable geometry, e.g. a sphere of radius $r = R$ in \mathbb{R}^3 , see Fig. 1. Using the Fourier transform $\phi(x, \omega)$ of the solution $\phi(x, t)$ defined as

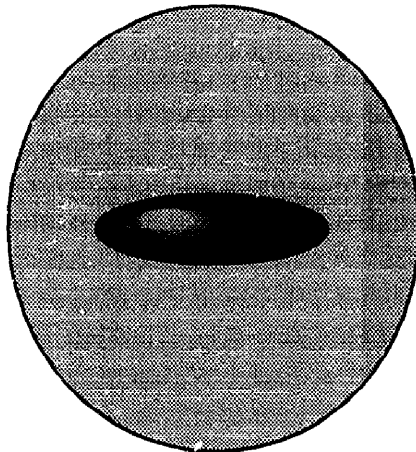


Fig. 1. Illustration of a finite computational domain enclosed by a spherical artificial boundary of radius R .

$$\tilde{\phi}(\mathbf{x}, \omega) := \frac{1}{\sqrt{2\pi}} \int_{-\infty}^{\infty} \phi(\mathbf{x}, t) e^{i\omega t} dt \quad (2)$$

where ω is the temporal transform parameter (circular frequency) and $i = \sqrt{-1}$, the exact DtN boundary condition can be expressed in terms of an infinite series of spherical wave harmonics as, see e.g. [2]:

$$\frac{\partial \tilde{\phi}}{\partial n}(R, \theta, \varphi) = \sum_{n=0}^{\infty} z_n(kR) \int_{\Gamma_x} s_n(\theta, \varphi, \theta', \varphi') \tilde{\phi}(R, \theta', \varphi') d\Gamma' \quad (3)$$

where the DtN kernels s_n , $n = 0, 1, 2, \dots$ are given by

$$s_n = \sum_{j=0}^n \alpha_{nj} P_n^j(\cos \varphi) P_n^j(\cos \varphi') \cos j(\theta - \theta') \quad (4)$$

$$\alpha_{nj} = \frac{(2n+1)(n-j)!}{2\pi R^2(n+j)!} \quad (5)$$

with impedance coefficients,

$$z_n(kR) = \frac{kh'_n(kR)}{h_n(kR)} \quad (6)$$

In the above, $k = \omega/c$ is the acoustic wavenumber, $0 \leq \theta < 2\pi$ is the circumferential angle and $0 \leq \varphi < \pi$ is the polar angle for a spherical truncation boundary of radius $r = R$. The differential surface area is $d\Gamma' = R^2 \sin \varphi' d\theta' d\varphi'$, P_n^j are associated Legendre functions of the first kind, and h_n are spherical Hankel functions of the first kind of order n . The prime on h_n indicates differentiation with respect to its argument, and the prime after the sum indicates that a factor of $1/2$ multiplies the term with $j = 0$. The boundary condition (3) can be written in operator form as

$$\frac{\partial \tilde{\phi}}{\partial n}(\mathbf{x}, k) = -\mathbb{S}(k) \tilde{\phi}(\mathbf{x}, k), \quad \mathbf{x} \in \Gamma_x \quad (7)$$

relating Dirichlet data, $\tilde{\phi}$, to Neumann data, $\partial \tilde{\phi} / \partial n$, through the linear mapping $\mathbb{S}(k): \tilde{\phi} \mapsto \partial \tilde{\phi} / \partial n$. This operator represents the exact impedance of the exterior domain restricted to Γ_x . The DtN map \mathbb{S} , is an integral operator resulting in a non-local boundary condition coupling all points on the artificial boundary Γ_x .

Local time-harmonic boundary conditions were derived by Givoli and Keller [4], where a spatially local counterpart to the non-local DtN map $\mathbb{S}(k)$ was obtained for the two-dimensional Helmholtz equation. The extension to three dimensions was given by Harari [5]. The derivation of local time-harmonic boundary conditions in the frequency domain starts by truncating the DtN map (3), so that the sum over n extends over the finite range $n = 0, 1, \dots, N-1$. The first N terms in the DtN map can be expressed as a finite series of spherical wave harmonics:

$$\frac{\partial \tilde{\phi}}{\partial n}(R, \theta, \varphi) = \sum_{n=0}^{N-1} z_n(kR) Y_n(\theta, \varphi) \quad (8)$$

where

$$Y_n(\theta, \varphi) = \sum_{j=0}^n P_n^j(\cos \varphi) (A_{nj} \cos j\theta + B_{nj} \sin j\theta) \quad (9)$$

are spherical surface harmonics of order n , with coefficients

$$A_{nj} = \alpha_{nj} \int_{\Gamma_\infty} \tilde{\phi}(R, \theta, \varphi) P_n^j(\cos \varphi) \cos j\theta \, d\Gamma \quad (10)$$

$$B_{nj} = \alpha_{nj} \int_{\Gamma_\infty} \tilde{\phi}(R, \theta, \varphi) P_n^j(\cos \varphi) \sin j\theta \, d\Gamma \quad (11)$$

The goal is to replace the non-local spatial integrals embedded in the coefficients A_{nj} and B_{nj} with local spatial derivatives. This can be accomplished by recognizing that the spherical harmonics Y_n can be interpreted as eigenfunctions of the Laplace–Beltrami operator

$$\Delta_r := \frac{1}{\sin \varphi} \frac{\partial}{\partial \varphi} \left(\sin \varphi \frac{\partial}{\partial \varphi} \right) + \frac{1}{\sin^2 \varphi} \frac{\partial^2}{\partial \theta^2} \quad (12)$$

with eigenvalues $\lambda = -n(n+1)$, i.e.

$$\Delta_r Y_n = -n(n+1) Y_n \quad (13)$$

so that

$$[n(n+1)]^m Y_n = (-\Delta_r)^m Y_n \quad (14)$$

This property of the spherical harmonics suggests writing the impedance coefficients as a series of powers of $n(n+1)$:

$$z_n(kR) = \sum_{m=0}^{N-1} [n(n+1)]^m \beta_m(kR), \quad n = 0, 1, \dots, N-1 \quad (15)$$

This is a system of N linear equations for the N unknown values β_m , $m = 0, 1, \dots, N$. Using (15) to replace z_n in (8) gives

$$\frac{\partial \tilde{\phi}}{\partial n}(R, \theta, \varphi) = \sum_{n=0}^{N-1} \sum_{m=0}^{N-1} \beta_m(kR) [n(n+1)]^m Y_n(\theta, \varphi) \quad (16)$$

Now using (14) to replace $[n(n+1)]^m Y_n$ with the high-order tangential derivatives $(-\Delta_r)^m Y_n$ results in

$$\frac{\partial \tilde{\phi}}{\partial n}(R, \theta, \varphi) = \sum_{n=0}^{N-1} \sum_{m=0}^{N-1} \beta_m(kR) (-\Delta_r)^m Y_n(\theta, \varphi) \quad (17)$$

After rearranging sums and using the assumption that the solution ϕ on Γ_∞ contains only the first N spherical harmonics, i.e.

$$\tilde{\phi}(R, \theta, \varphi) = \sum_{n=0}^{N-1} Y_n(\theta, \varphi) \quad (18)$$

the following sequence of local radiation boundary conditions is obtained,

$$\frac{\partial \tilde{\phi}}{\partial n} = \sum_{m=0}^{N-1} \beta_m(kR) (-\Delta_r)^m \tilde{\phi} \quad \text{on } \Gamma_\infty \quad (19)$$

In (19), the values of $\beta_m(kR)$ are obtained by solving the $N \times N$ linear algebraic system (15). Since this sequence follows directly from the truncated DtN map, these radiation boundary operators are exact for waves consisting of the first N spherical harmonics. In this case, the non-local spatial integrals have been replaced by a linear map expressed in terms of the differential operator $(\Delta_r)^m$.

3. New exact time-dependent boundary conditions

A direct inverse transform of $\mathbb{S}(k)$ from the frequency domain to the time domain results in a time convolution of the form,

$$\frac{\partial \phi}{\partial n}(x, t) = \int_0^t \mathbb{S}(t - \tau) \phi(\tau) d\tau \quad x \in \Gamma_x \quad (20)$$

This boundary condition is non-local in both x and t . In order to circumvent the difficulty of having to implement a temporal convolution integral, time-dependent boundary conditions are derived which replace the temporal integral with local temporal derivatives. In this way, the boundary conditions at time t will involve only the values of the solution and its derivatives at time t , and not values at previous times. Two alternative sequences are derived; the first involves time derivatives yet retains the spatial integral of the DtN map (local in time and non-local in space version), and the second involves both time and spatial derivatives (local in time and local in space version). Throughout the development, we use the special property of spherical Hankel functions h_n which have the unique feature of being exactly represented by a finite and convergent series up to order n (see e.g. [13])

$$h_n(kR) = h_0(kR) \left[(-i)^n \sum_{j=0}^n \frac{(n+j)!}{j!(n-j)!} \left(\frac{-1}{2ikR} \right)^j \right], \quad n = 0, 1, 2, \dots \quad (21)$$

As this series involves only the zero-order term $h_0 = e^{ikR}/(ikR)$ multiplied by a sum over inverse powers of the non-dimensional wavenumber (ikR) , an inverse Fourier transform can be found which yields a local in time counterpart to the DtN map.

A finite series representation for the cylindrical Hankel functions H_n appearing in the two-dimensional DtN map is not available. In this case an alternative approach based on an asymptotic expansion is necessary for the development of boundary conditions that are local in time t (see [14]).

3.1. Local in time and non-local in space version

In order to obtain non-reflecting boundary conditions which possess the important property of locality in time, without the requirement of high-order tangential continuity in the Laplace–Beltrami operator $(\Delta_\Gamma)^j$, a local in time counterpart to the spatially non-local DtN map (3) is derived which exactly represents the first N spherical wave harmonics. This new sequence of boundary conditions retains the non-local spatial integral, while replacing the temporal integral of the time-convoluted DtN map with higher-order local time derivatives. This new sequence of time-dependent boundary conditions has the advantage that when implemented in the time-discontinuous finite element formulation, standard $C^0(\Gamma_x \times I_n)$ interpolation functions may be used for both the space and time dimensions.

First-order boundary condition

For clarity, set $h_n := h_n(kR)$, and consider the first term in the truncated DtN series with $N = 1$, then (3) reduces to

$$\frac{\partial \tilde{\phi}}{\partial n} = z_0 \int_{\Gamma_x} \tilde{\phi} s_0 d\Gamma' \quad (22)$$

where $s_0 = 1/(4\pi R^2)$ and $z_0 = kh_0'/h_0$. Using $h_0' = -h_1$ and (21) and clearing the denominator h_0 gives the alternate form,

$$\frac{\partial \tilde{\phi}}{\partial n} = \left(ik - \frac{1}{R} \right) \int_{\Gamma_x} \tilde{\phi} s_0 d\Gamma' \quad (23)$$

The time-dependent counterpart to (23) is obtained by direct application of the inverse Fourier transform:

$$\phi(\mathbf{x}, t) := \frac{1}{\sqrt{2\pi}} \int_{-\infty}^{\infty} \tilde{\phi}(\mathbf{x}, \omega) e^{-i\omega t} d\omega \tag{24}$$

in effect, replacing every occurrence of the operator $(-ik)^m$ by $(1/c \partial/\partial t)^m$ with the result,

$$\mathbb{B}_1 \phi := \frac{\partial \phi}{\partial n} + \int_{\Gamma'} \left(\frac{1}{c} \dot{\phi} + \frac{1}{R} \phi \right) s_0 d\Gamma' = 0 \tag{25}$$

This operator is local in time and non-local in space and is perfectly absorbing for axially symmetric spherical waves (outgoing wave harmonic $n = 0$).

Second-order boundary condition

For $N = 2$, the first two terms in the truncated DtN series (3) take the form,

$$\frac{\partial \tilde{\phi}}{\partial n} = z_0 \int_{\Gamma'} \tilde{\phi} s_0 d\Gamma' + z_1 \int_{\Gamma'} \tilde{\phi} s_1 d\Gamma' \tag{26}$$

Using the definition for $z_n(kR)$, the recurrence relation,

$$h'_n = h_{n-1} - \left(\frac{n+1}{kR} \right) h_n, \quad n = 1, 2, \dots \tag{27}$$

in conjunction with (21), and clearing the common denominator $h_0 h_1$ we obtain the alternative form,

$$\left(\frac{1}{R} - ik \right) \frac{\partial \tilde{\phi}}{\partial n} = \left(k^2 + \frac{2ik}{R} - \frac{1}{R^2} \right) \int_{\Gamma'} \tilde{\phi} s_0 d\Gamma' + \left(k^2 + \frac{2ik}{R} - \frac{2}{R^2} \right) \int_{\Gamma'} \tilde{\phi} s_1 d\Gamma' \tag{28}$$

Direct application of the inverse Fourier transform gives

$$\mathbb{B}_2 \phi := \frac{\partial \phi}{\partial n} + \frac{R}{c} \frac{\partial \dot{\phi}}{\partial n} + \int_{\Gamma'} \left(\frac{R}{c^2} \ddot{\phi} + \frac{2}{c} \dot{\phi} + \frac{1}{R} \phi \right) s_0 d\Gamma' + \int_{\Gamma'} \left(\frac{R}{c^2} \ddot{\phi} + \frac{2}{c} \dot{\phi} + \frac{2}{R} \phi \right) s_1 d\Gamma' = 0 \tag{29}$$

where s_0 and s_1 are defined in (4). This condition is perfectly absorbing for the first two spherical wave harmonics of order $n = 0$ and $n = 1$.

Third-order boundary condition

Following the same procedure, for $N = 3$, the first three terms in the truncated DtN series (3) are

$$\frac{\partial \phi}{\partial n} = z_0 \int_{\Gamma'} \phi s_0 d\Gamma' + z_1 \int_{\Gamma'} \phi s_1 d\Gamma' + z_2 \int_{\Gamma'} \phi s_2 d\Gamma' \tag{30}$$

Using the definition for z_n , the relations (21), (27) and clearing the common denominator $h_0 h_1 h_2$ we obtain the alternative form,

$$\gamma_0 \frac{\partial \phi}{\partial n} = \gamma_1 \int_{\Gamma'} \phi s_0 d\Gamma' + \gamma_2 \int_{\Gamma'} \phi s_1 d\Gamma' + \gamma_3 \int_{\Gamma'} \phi s_2 d\Gamma' \tag{31}$$

where

$$\begin{aligned} \gamma_0 &= 1 - 2ikR - 4(kR)^2/3 + i(kR)^3/3 \\ \gamma_1 &= -1/R + 3ik + 10k^2R/3 - 5ik^3R^2/3 - k^4R^3/3 \\ \gamma_2 &= -2/R + 4ik + 11k^2R/3 - 5ik^3R^2/3 - k^4R^3/3 \\ \gamma_3 &= -3/R + 6ik + 13k^2R/3 - 5ik^3R^2/3 - k^4R^3/3 \end{aligned}$$

Taking the inverse Fourier transform gives the time-dependent counterpart:

$$\begin{aligned} \mathbb{B}_3\phi := & \phi_{,n} + \frac{2R}{c}\phi_{,nt} + \frac{4R^2}{3c^2}\phi_{,nnt} + \frac{R^3}{3c^3}\phi_{,nnnt} \tag{32} \\ & + \int_{\Gamma_x} \left(\frac{R^3}{3c^4}\phi_{,nnnt} + \frac{5R^2}{3c^3}\phi_{,nnt} + \frac{10R}{3c^2}\phi_{,nt} + \frac{3}{c}\phi_{,t} + \frac{1}{R}\phi \right) s_0 \, d\Gamma' \\ & + \int_{\Gamma_x} \left(\frac{R^3}{3c^4}\phi_{,nnnt} + \frac{5R^2}{3c^3}\phi_{,nnt} + \frac{11R}{3c^2}\phi_{,nt} + \frac{4}{c}\phi_{,t} + \frac{2}{R}\phi \right) s_1 \, d\Gamma' \\ & + \int_{\Gamma_x} \left(\frac{R^3}{3c^4}\phi_{,nnnt} + \frac{5R^2}{3c^3}\phi_{,nnt} + \frac{13R}{3c^2}\phi_{,nt} + \frac{6}{c}\phi_{,t} + \frac{3}{R}\phi \right) s_2 \, d\Gamma' = 0 \tag{33} \end{aligned}$$

where $s_n, n = 0, 1, 2$ are defined in (4). This condition is perfectly absorbing for the first three spherical wave harmonics of order $n = 0, 1, 2$. Local in time counterparts for the higher terms, $N \geq 4$, in the truncated DtN series are obtained following the same procedure outlined for $N = 1, 2, 3$. These are non-local operators that involve a spatial integral yet retain the important property of locality in time. In general, the boundary operators in the sequence will have higher-order time derivatives up to $2(N - 1)$.

When implemented in the discontinuous space–time element formulation, [7], with time step interval $I_n =]t_n, t_{n+1}[$, standard $C^0(\Gamma_x \times I_n)$ continuous interpolations may be used on the radiation boundary in both the space and time dimensions. For example, for the third-order operator \mathbb{B}_3 defined in (33), standard $C^0(I_n)$ quartic basis functions in the time dimension and $C^0(\Gamma_x)$ linear basis functions in the spatial dimension may be used to interpolate the fourth-order temporal and first-order spatial derivatives appearing in the boundary operator. This feature circumvents the need for high-order continuous tangential interpolation functions.

3.2. Local in time and local in space version

To derive a sequence of non-reflecting boundary conditions which are local in both time t and space x , yet retains the desirable property of being exact for the first N outgoing spherical wave harmonics, we replace the space–time convolution integral in (20) with local temporal and spatial derivatives. The development proceeds by deriving an exact time-dependent counterpart to the local time-harmonic DtN given in (19), through use of an inverse Fourier transform and the finite series expansion (21) for the spherical Hankel functions embedded in the coefficients β_m .

First-order boundary condition

For the first operator in the sequence corresponding to $N = 1$, the system (15) reduces to the simple result $z_0(kR) = \beta_0(kR)$, so that the local DtN condition (19) specializes to

$$\frac{\partial \tilde{\phi}}{\partial n} = \frac{kh'_0(kR)}{h_0(kR)} \tilde{\phi} \tag{34}$$

Using the relation $h'_0 = -h_1$ and (21) with $n = 1$, i.e.

$$h_1 = \left(\frac{1}{kR} - i \right) h_0 \tag{35}$$

we obtain a simplified expression for (34):

$$\frac{\partial \tilde{\phi}}{\partial n} = \left(ik - \frac{1}{R} \right) \tilde{\phi} \tag{36}$$

Taking the inverse Fourier transform we obtain the local in time and space operator,

$$\mathbb{B}_1\phi := \frac{\partial\phi}{\partial n} + \frac{1}{R}\phi + \frac{1}{c}\dot{\phi} = 0 \quad (37)$$

This condition is perfectly absorbing for only axially symmetric spherical waves (outgoing wave harmonic $n = 0$).

Second-order boundary condition

To obtain a high-order accurate boundary condition, take $N = 2$, so that the system (15) yields, $\beta_0 = z_0$ and $\beta_1 = (z_1 - z_0)/2$, and (19) becomes

$$\frac{\partial\tilde{\phi}}{\partial n} = z_0\phi + \frac{1}{2}(z_0 - z_1)\Delta_r\tilde{\phi} \quad (38)$$

Clearing the common denominator h_0h_1 we obtain

$$h_0h_1\frac{\partial\tilde{\phi}}{\partial n} = (kh'_0h_1)\tilde{\phi} + \frac{k}{2}(h'_0h_1 - h'_1h_0)\Delta_r\tilde{\phi} \quad (39)$$

Using the recurrence relation (27), in conjunction with (21) and after some algebraic manipulation, we obtain the simplified form,

$$\left(\frac{1}{R} - ik\right)\frac{\partial\tilde{\phi}}{\partial n} = \left(k^2 + \frac{2ik}{R} - \frac{1}{R^2}\right)\tilde{\phi} + \frac{1}{2R^2}\Delta_r\tilde{\phi} \quad (40)$$

Since this expression involves only terms in powers of $(ik)^m$, the inverse Fourier transform is readily obtained with the desired result,

$$\mathbb{B}_2\phi := \frac{\partial\phi}{\partial n} + \frac{R}{c}\frac{\partial\dot{\phi}}{\partial n} + \frac{R}{c^2}\ddot{\phi} + \frac{2}{c}\dot{\phi} + \frac{1}{R}\phi - \frac{1}{2R}\Delta_r\phi = 0 \quad (41)$$

This higher-order accurate local boundary condition is perfectly absorbing for the first two spherical wave harmonics of orders $n = 0$ and $n = 1$.

Third-order boundary condition

Proceeding in the same fashion with $N = 3$, (19) becomes

$$\frac{\partial\tilde{\phi}}{\partial n} = \beta_0\tilde{\phi} - \beta_1\Delta_r\tilde{\phi} + \beta_2(\Delta_r)^2\tilde{\phi} \quad (42)$$

and the system (15) yields the three coefficients,

$$\begin{aligned} \beta_0 &= z_0 \\ \beta_1 &= (18z_1 - 16z_0 - 2z_2)/24 \\ \beta_2 &= (2z_0 + z_2 - 3z_1)/24 \end{aligned}$$

Using the recurrence relation (27) in conjunction with (21), or equivalently

$$h_{n+1} = \frac{(2n+1)}{kR}h_n - h_{n-1}, \quad n = 1, 2, \dots \quad (43)$$

we obtain the simplified form,

$$\gamma_0\tilde{\phi}_{,n} = \gamma_1\tilde{\phi} + \gamma_2\Delta_r\tilde{\phi} + \gamma_3(\Delta_r)^2\tilde{\phi} \quad (44)$$

where the frequency-dependent coefficients are

$$\begin{aligned} \gamma_0 &= 1 - 2ikR - 4(kR)^2/3 + i(kR)^3/3 \\ \gamma_1 &= -1/R + 3ik + 10k^2R/3 - 5ik^3R^2/3 - k^4R^3/3 \\ \gamma_2 &= 7/(12R) - ik/2 - k^2R/6 \\ \gamma_3 &= 1/(24R) \end{aligned}$$

Direct application of the inverse transform gives

$$\begin{aligned} \mathbb{B}_3\phi := & \phi_{,n} + \frac{2R}{c}\phi_{,nt} + \frac{4R^2}{3c^2}\phi_{,nnt} + \frac{R^3}{3c^3}\phi_{,nnnt} + \frac{1}{R}\phi + \frac{3}{c}\phi_{,t} + \frac{10R}{3c^2}\phi_{,tt} + \frac{5R^2}{3c^3}\phi_{,ttt} + \frac{R^3}{3c^4}\phi_{,tttt} \\ & - \frac{7}{12R}\Delta_r\phi - \frac{1}{2c}\Delta_r\phi_{,t} - \frac{R}{6c^2}\Delta_r\phi_{,tt} - \frac{1}{24R}(\Delta_r)^2\phi = 0 \end{aligned} \tag{45}$$

In this expression a comma denotes differentiation. This higher-order accurate local boundary condition is perfectly absorbing for the first three spherical wave harmonics of orders $n=0, 1$ and $n=2$. Expressions for the exact time-dependent local boundary conditions for higher-order harmonics $N=4, 5, \dots$, will involve higher-order temporal and tangential derivatives, and are obtained using the same procedure as indicated for $N=1, 2, 3$.

This new sequence of local time-dependent boundary conditions provide increasing accuracy with order N which, however, is also a measure of the difficulty of implementation. In general, the N th-order condition contains all the even tangential and temporal derivatives up to order $2(N-1)$. Because the time-discontinuous formulation allows for the use of $C^0(I_n)$ interpolations in time to represent the high-order time derivatives, in principle it is possible to implement this sequence of time-dependent absorbing boundary conditions up to the order dictated by the time-derivatives appearing in the boundary operator.

The implementation of \mathbb{B}_1 and \mathbb{B}_2 are straightforward. For example, for the operator \mathbb{B}_2 defined in (41), the second-order time derivative may be approximated in the time-discontinuous method by $C^0(I_n)$ quadratic interpolations in time, while the high-order $C^1(\Gamma_x)$ continuity implied by the second-order tangential derivatives embedded in the Laplace–Beltrami operator Δ_r can be relaxed to $C^0(\Gamma_x)$ through integration by parts in the spatial dimension over the closed surface Γ_x .

However, for high-order operators in the sequence extending beyond $N \geq 3$, the lowest possible order of spatial continuity on the artificial boundary that can be achieved after integration by parts is C^{N-2} . For these high-order operators a layer of boundary elements adjacent to Γ_x , possessing high-order tangential continuity on Γ_x are needed. For example, for the \mathbb{B}_3 operator defined in (45), $C^1(\Gamma_x)$ continuous interpolation functions, e.g. Hermite polynomials, are needed to represent the second-order tangential derivatives appearing in the weak enforcement of \mathbb{B}_3 .

An interesting observation is that the first-order operator \mathbb{B}_1 coincides with the well known spherical damper and is equivalent to the first local boundary condition in the sequence derived by Bayliss and Turkel [11] and Engquist and Majda [9]. In addition, we observe that the local boundary condition \mathbb{B}_2 defined in (41), which is exact for the first two spherical wave harmonics, coincides with the second-order boundary condition derived by Bayliss and Turkel [11], after the higher-order radial derivatives in the Bayliss and Turkel sequence are eliminated in favor of high-order tangential derivatives through use of the wave equation in three dimensions. While the boundary conditions derived by Bayliss and Turkel were obtained by annihilating radial terms in a multipole expansion, it is seen, that in fact, the first two boundary conditions in the sequence share the property of the localized DtN, in that they match the first two spherical harmonics for outgoing waves on a spherical boundary Γ_x . The equivalence of this second-order operator holds in both the time-dependent and time-harmonic cases. However, for higher-order boundary conditions in the sequence beyond $N \geq 3$, the form of the proposed non-reflecting boundary conditions are different than those of Bayliss and Turkel.

4. Space-time finite element implementation

A direct approach in which to implement the exact time-dependent boundary condition is to define a linear operator \mathbb{S}_m as

$$\mathbb{B}_m(\phi) := \frac{\partial \phi}{\partial n} + \mathbb{S}_m(\phi) \quad (46)$$

which implies

$$\frac{\partial \phi}{\partial n} = -\mathbb{S}_m \phi \quad \text{on } \Gamma, \quad (47)$$

In this way, the boundary conditions are expressed in a form relating Dirichlet-to-Neumann data. For example, the first three local in space and time operators \mathbb{S}_m for m equal to 1, 2 and 3 are:

$$\mathbb{S}_1 \phi = \frac{1}{R} \phi + \frac{1}{c} \phi_t, \quad (48)$$

$$\mathbb{S}_2 \phi = \frac{1}{2R} (2 - \Delta_r) \phi + \frac{1}{c} \left(2 + R \frac{\partial}{\partial r} \right) \phi_t + \frac{R}{c^2} \phi_{tt}, \quad (49)$$

$$\begin{aligned} \mathbb{S}_3 \phi = & \frac{1}{24R} (24 - 14\Delta_r - (\Delta_r)^2) \phi + \frac{1}{2c} \left(6 - \Delta_r + 4R \frac{\partial}{\partial r} \right) \phi_t \\ & + \frac{R}{6c^2} \left(20 - \Delta_r + 8R \frac{\partial}{\partial r} \right) \phi_{tt} + \frac{R^2}{3c^3} \left(5 + R \frac{\partial}{\partial r} \right) \phi_{ttt} + \frac{R^3}{3c^4} \phi_{tttt} \end{aligned} \quad (50)$$

In general, the linear mapping $\mathbb{S}_m \phi$ takes the form

$$\mathbb{S}_m \phi = \sum_{j=0}^m C_j \left[\frac{\partial^j \phi}{\partial t^j} \right] \quad \text{on } Y_x := \Gamma_x \times I_n \quad (51)$$

where C_j , $j=0, 1, \dots, m$, represent spatial operators that may be local differential operators that couple only adjacent points on the artificial boundary, or non-local integral operators that couple all points on the artificial boundary Γ_x . This sequence of boundary operators can be incorporated into the space-time finite element formulation as natural boundary conditions, where they are weakly enforced in both time and space as described in Part I [7]. Here, we recall the time-discontinuous Galerkin variational equation for acoustics; for simplicity only the variational equation for the acoustic fluid with the radiation boundary operator on the artificial truncation boundary Γ_x is stated.

For the acoustic problem, within each space-time slab, $n=0, 1, \dots, N-1$, the objective is to find $\phi^h \in \mathcal{F}_n^h$, such that $\forall w^h \in \mathcal{W}_n^h$, the following equation is satisfied,

$$E_t(w^h, \phi^h)_n + E_r(w^h, \phi^h)_n = L_t(w^h)_n \quad (52)$$

In this space-time variational equation, $\phi^h \in \mathcal{F}_n^h$ is the space-time finite element trial solution with corresponding weighting function $w^h \in \mathcal{W}_n^h$. We recall from Part I that for the time-discontinuous method, the space of trial solutions \mathcal{F}_n^h are C^0 continuous polynomials defined over the space-time domain $Q_n^I = \Omega_t \times I_n$ and radiation boundary $Y_x = \Gamma_x \times I_n$, with time step interval $I_n =]t_n, t_{n+1}[$.

The operator

$$E_t(w^h, \phi^h)_n := (w^h, a^2 \dot{\phi}^h)_{Q_n^I} + (\nabla w^h, \nabla \phi^h)_{Q_n^I} + (w^h(t_n^+), a^2 \dot{\phi}^h(t_n^+))_{\Omega_t} + (\nabla w^h(t_n^+), \nabla \phi^h(t_n^+))_{\Omega_t} \quad (53)$$

with notation for inner products,

$$(w^h, \phi^h)_{\Omega_t} = \int_{\Omega_t} \rho_0 w^h \phi^h \, d\Omega \quad (54)$$

$$(\nabla w^h, \nabla \phi^h)_{\Omega_t} = \int_{\Omega_t} \rho_0 \nabla w^h \cdot \nabla \phi^h \, d\Omega \quad (55)$$

$$(w^h, \phi^h)_{Q_n^f} = \int_{t_n}^{t_{n+1}} (w^h, \phi^h)_{\Omega_t} dt \tag{56}$$

acts to weakly enforce the second-order hyperbolic wave equation within a space–time slab Q_n^f and together with the forcing operator $L_t(w^h)_n$ acts to weakly enforce the continuity of the solution across time slabs.

Non-reflecting boundary conditions are weakly enforced through the radiation boundary operator $E_r(w^h, \phi^h)_n$. For absorbing boundary conditions up to second-order ($m = 2$), the variational equation for the radiation boundary can be written in abstract form as

$$E_r(w^h, \phi^h)_n := (w^h, \mathbb{S}_m \phi^h)_{(Y_x)_n} + d_2(\dot{w}^h(t_n^+), \llbracket \dot{\phi}^h(t_n) \rrbracket)_{\Gamma_x} + d_0(w^h(t_n^+), \llbracket \phi^h(t_n) \rrbracket)_{\Gamma_x} \tag{57}$$

for $m = 1$ or $m = 2$ where we have used the notation for the weighted L_2 products on Γ_x as

$$(w^h, \phi^h)_{\Gamma_x} = \int_{\Gamma_x} \rho_0 w^h \phi^h d\Gamma \tag{58}$$

$$(w^h, \phi^h)_{(Y_x)_n} = \int_{t_n}^{t_{n+1}} (w^h, \phi^h)_{\Gamma_x} dt \tag{59}$$

The term evaluated over $(Y_x)_n := \Gamma_x \times I_n$ acts to weakly enforce the non-reflecting boundary condition (47) over the time interval $]t_n, t_{n+1}[$ and Γ_x . As a specific example, consider the second-order \mathbb{S}_2 , non-reflecting boundary condition defined previously in (49): In this case, the acoustic radiation operator takes the form

$$(w^h, \mathbb{S}_2 \phi^h)_{(Y_x)_n} := d_0(\dot{w}^h, \phi^h)_{(Y_x)_n} + d_1(\dot{w}^h, \dot{\phi}^h)_{(Y_x)_n} + d_2(\dot{w}^h, \ddot{\phi}^h)_{(Y_x)_n} \tag{60}$$

where

$$d_0(\dot{w}^h, \phi^h)_{(Y_x)_n} = \frac{1}{R} (\dot{w}^h, \phi^h)_{(Y_x)_n} + \frac{1}{2R} (\dot{w}^h_{,\varphi}, \phi^h_{,\varphi})_{(Y_x)_n} + \frac{1}{2R} (\dot{w}^h_{,\theta}, \csc^2(\varphi) \phi^h_{,\theta})_{(Y_x)_n} \tag{61}$$

$$d_1(\dot{w}^h, \dot{\phi}^h)_{(Y_x)_n} = \frac{2}{c} (\dot{w}^h, \dot{\phi}^h)_{(Y_x)_n} + \frac{R}{c} (\dot{w}^h, \dot{\phi}^h_{,r})_{(Y_x)_n} \tag{62}$$

$$d_2(\dot{w}^h, \ddot{\phi}^h)_{(Y_x)_n} = \frac{R}{c^2} (\dot{w}^h, \ddot{\phi}^h)_{(Y_x)_n} \tag{63}$$

In (61), tangential continuity is relaxed on the boundary Γ_x through integration by parts:

$$(w, \Delta_T \phi)_{\Gamma_x} = - (w_{,\varphi}, \phi_{,\varphi})_{\Gamma_x} - (w_{,\theta}, \csc^2(\varphi) \phi_{,\theta})_{\Gamma_x} \tag{64}$$

For this boundary condition, C^0 continuous interpolations are sufficient in both space and time. Since these boundary operators are local in space and time, when implemented with standard finite element interpolations with compact support, the boundary integrals couple only degrees-of-freedom in adjacent elements, and the banded sparse data structure of the finite element arrays are preserved. The locality in time enables the use of updates from one time step t_n to the next t_{n+1} without storage of data from any previous time $t_{n-1}, t_{n-2}, \dots, t_0$. Thus, local in time boundary conditions of this type have a distinct advantage in computational storage when compared to competing approaches, e.g. the use of Kirchoff's retarded potential or the direct convolution of the DtN map (20), which involves a temporal integral over all past time and leads to numerical formulations that can be extremely memory-intensive, typically requiring storage of a large pool of historical data.

The operators $d_2(\cdot, \cdot)_{\Gamma_x}$ and $d_0(\cdot, \cdot)_{\Gamma_x}$ evaluated over the space–time slab interface at the boundary Γ_x in (57) act to weakly enforce continuity of the trial solution across space–time slab interfaces, and are designed to be consistent with the radiation boundary operator (60) evaluated over $(Y_x)_n$. Thus, the

form of the consistent temporal jump operators $\llbracket \phi^h(t_n) \rrbracket$ and $\llbracket \dot{\phi}^h(t_n) \rrbracket$ embedded in the last two terms of (57) depend on the form of the spatial derivatives appearing in the bilinear operators $d_0(\cdot, \cdot)_{(\Gamma_x)_n}$ and $d_2(\cdot, \cdot)_{(\Gamma_x)_n}$ defined in (61) and (63). For example, for the local boundary condition (49), the consistent jump terms specialize to

$$d_0(w^h(t_n^*), \llbracket \phi^h(t_n) \rrbracket)_{\Gamma_x} = \frac{1}{R} (w^h(t_n^*), \llbracket \phi^h(t_n) \rrbracket)_{\Gamma_x} + \frac{1}{2R} (w_{,\varphi}^h(t_n^*), \llbracket \phi_{,\varphi}^h(t_n) \rrbracket)_{\Gamma_x} + \frac{1}{2R} (w_{,\theta}^h(t_n^*), \csc^2(\varphi) \llbracket \phi_{,\theta}^h(t_n) \rrbracket)_{\Gamma_x} \tag{65}$$

$$d_2(w^h(t_n^*), \llbracket \dot{\phi}^h(t_n) \rrbracket)_{\Gamma_x} = \frac{R}{c^2} (w^h(t_n^*), \llbracket \dot{\phi}^h(t_n) \rrbracket)_{\Gamma_x} \tag{66}$$

As discussed in Part 1, these consistent temporal jump operators are required for the unconditional stability of the formulation. A numerical example demonstrating the importance of this stability requirement will given in Section 5.4.

REMARK 1. An alternate implementation of the exact time-dependent non-reflecting boundary conditions which avoids approximation of the radial derivative on Γ_x , is possible. This alternative implementation is based on the procedure used by Kallivokas et al. [15] for the symmetrization of a second-order absorbing boundary condition in a standard semidiscrete finite element method. Multiplying the boundary operator (41) by $\alpha = c/R$ and recognizing the hierarchical structure inherent in \mathbb{B}_2 , we can express (41) in the alternative form

$$\alpha \phi_{,n} + \dot{\phi}_{,n} = -\alpha \mathbb{S}_1 \phi - \mathbb{S}_1 \dot{\phi} + \frac{\alpha}{2R} \Delta_r \phi \tag{67}$$

where \mathbb{S}_1 is the first-order boundary operator defined in (48). By introducing an auxiliary variable ψ on Γ_x , the boundary condition (67) can be split into the following equivalent system of two equations:

$$\begin{aligned} \phi_{,n} &= -\mathbb{S}_1 \phi + \frac{1}{2R} \Delta_r \psi \\ \frac{1}{2R} \Delta_r \phi &= \frac{1}{2} \mathbb{S}_1 \Delta_r \psi \end{aligned} \tag{68}$$

After implementing (68) in the time-discontinuous Galerkin variational equation (52), the resulting expression for the radiation operator $E_r(\cdot, \cdot)_n$ involves only spatially symmetric terms, thus avoiding the spatially non-symmetric operator of (62) appearing in the direct implementation of \mathbb{B}_2 ; albeit at the extra expense of having to solve for an additional auxiliary variable on Γ_x .

REMARK 2. An alternative form of our boundary conditions \mathbb{B}_m , $m = 1, 2, \dots$ for both the local in space and non-local in space versions can be obtained by replacing the high-order temporal derivatives appearing in the operator with high-order radial and tangential derivatives through repeated use of the wave equation written in separable coordinates, e.g. for a sphere in three dimensions,

$$\frac{\partial^2 \phi}{\partial t^2} = \left(\frac{c}{r}\right)^2 \left[\frac{\partial}{\partial r} \left(r^2 \frac{\partial \phi}{\partial r} \right) + \Delta_r \phi \right] \tag{69}$$

evaluated at $r = R$. However, in this approach the implementation of high-order radial derivatives is not natural to the standard finite element method, and is not recommended.

5. Numerical examples

In this section a number of numerical examples are described to demonstrate the effectiveness of the time-discontinuous Galerkin space–time finite element method to accurately model transient acoustic

radiation. Only results for the local in time and local in space version of our exact non-reflecting boundary conditions defined in Section 3.2 are presented in this paper. The results of the new formulation are compared using the simple PW-damper \mathbb{S}_0 defined in (1), and the first-order \mathbb{S}_1 , and second-order \mathbb{S}_2 , local boundary conditions defined in (48) and (49), respectively. For all the numerical results presented, the GLS mesh parameters are set to zero and standard C^0 quadratic finite element shape functions are used in both the time and space dimensions.

To our knowledge, this is the first implementation of the time-discontinuous Galerkin space-time finite element method for second-order hyperbolic equations in multidimensions. Numerical results for one-dimensional problems (without non-reflecting boundaries) are reported in [16, 17]. In general, space-time methods give rise to a larger system of equations than those produced by typical semidiscrete methods. For the relatively small canonical examples presented, solutions were obtained using a direct Crout elimination solver with profile storage and dynamic memory allocation. Profile reduction based on a modified version of the reverse Cuthill–McKee algorithm was used to minimize storage (see Algorithm 582 in ACM-Trans. Math. Software, Vol. 8, No. 2). For larger problems, more efficient solution strategies are needed.

5.1. Spherical harmonic radiation

In order to assess the accuracy of the local non-reflecting boundary conditions, a series of numerical experiments are performed. These examples are designed to test the ability of the local boundary conditions to transmit outgoing spherical wave harmonics on the artificial boundary Γ_r . By driving the transient solution to steady-state, we are able to isolate the effect of each frequency on the accuracy of the absorbing boundary conditions.

Consider the time-harmonic radiation from a sphere of radius $r = a$, with a surface excitation driven by a spherical harmonic distribution of the form,

$$\phi(a, \varphi, t) = P_n(\cos \varphi) \sin \omega t, \quad \text{for } 0 \leq \varphi < \pi, \quad t > 0 \quad (70)$$

with homogeneous initial conditions. After the solution is driven to steady-state, the exact solution to this problem is

$$\phi(r, \varphi, t) = -\text{Imag} \left\{ \frac{h_n(kr)}{h_n(ka)} P_n(\cos \varphi) e^{-i\omega t} \right\} \quad \text{for } r \geq a \quad (71)$$

where P_n are Legendre polynomials of the first kind and h_n are spherical Hankel functions of the first kind of order n . When using a finite element method incorporating approximate absorbing boundary conditions on a spherical artificial boundary as illustrated in Fig. 2, this problem becomes increasingly difficult to solve as the wave harmonic n increases. Recall that the spherically symmetric damper \mathbb{S}_1 defined in (48) is exact for the breathing mode, which corresponds to $n = 0$ in (70). However, for higher modes, $n = 1, 2, \dots$ this low-order boundary condition is only approximate. An improved approximation is obtained by using the second-order operator \mathbb{S}_2 derived in (49). This time-dependent boundary condition is exact for the first two spherical harmonics, $n = 0, 1$.

A series of transient space-time finite element solutions were obtained for the loading in (70) with harmonics ranging from $n = 0$ through $n = 5$. The system starts from rest and is driven towards the steady-state solution with time, with a time-increment of $\Delta t = 0.1$ s. Due to the axisymmetric nature of the problem, the computational domain is taken as $\Omega = \{a < r < R, 0 \leq \varphi < \pi\}$, and the radiation boundary is set at $R = 2a$. The resulting bounded domain Ω is discretized with 400 axisymmetric acoustic elements: 10 elements in the radial direction, and 40 elements in the polar direction as indicated in Fig. 3. For this axisymmetric problem, there is no circumferential dependence on the solution and all terms which depend on the coordinate θ are neglected in the definition of the non-reflecting boundary conditions. In particular, for the local boundary operator \mathbb{S}_2 defined in (49), the third term in (61) and (65) involving derivatives with respect to θ are not used.

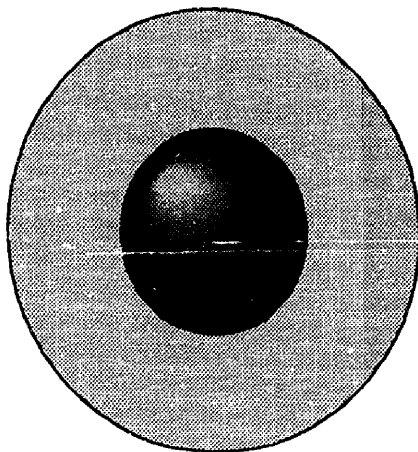


Fig. 2. Sphere of radius $r = a$ enclosed by a spherical artificial boundary of radius $R = 2a$.

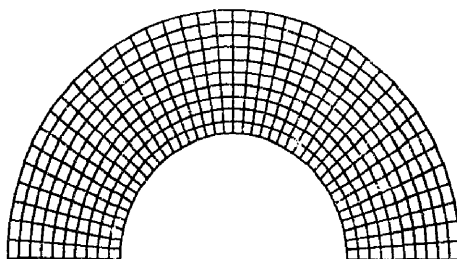


Fig. 3. Axisymmetric mesh with 400 quadratic elements.

Results for two different frequencies, $ka = 1$ and $ka = 3$, normalized with respect to the wave speed c and radius a are presented. The solution profile on the radiation boundary $r = 2a$ together with a plot along a radial line at the axis of symmetry are presented to obtain a quantitative estimate of the accuracy of the non-reflecting boundary operators. The time-history at a representative point on the absorbing boundary is also used as a quantitative measure of the error of the approximation. Finally, contour plots of the velocity potential are presented to study the global character of the solution.

Numerical solutions for the radiation loading $P_0(\cos \varphi) \sin \omega t$, confirmed that both the operators \mathbb{S}_1 , and \mathbb{S}_2 are exact for the first 'breathing' mode $n = 0$. To verify that the second-order boundary operator \mathbb{S}_2 is exact for the second wave harmonic, $n = 1$, numerical solutions are obtained for the loading $P_1(\cos \varphi) \sin \omega t$ and a non-dimensional frequency $\omega a/c = 1$. Fig. 4 shows the solution profile around the artificial boundary, together with the solution plotted along a radial line located at the polar angle $\varphi = 0$, both plotted at time $t = 20$. This sample time is sufficient in length so that the solution has reached steady-state, and is such that many spurious reflections between the artificial boundary $r = R$, and the radiating surface at $r = a$, could have occurred. The time-dependent solution at a point on the artificial boundary at position $(r, \varphi) = (R, 0)$ is given in Fig. 9 (top). These results confirm that the local operator \mathbb{S}_2 , when implemented in the space-time formulation gives nearly exact solutions for waves composed of spherical harmonics up to order $n = 1$. In contrast, the numerical solution using \mathbb{S}_1 is

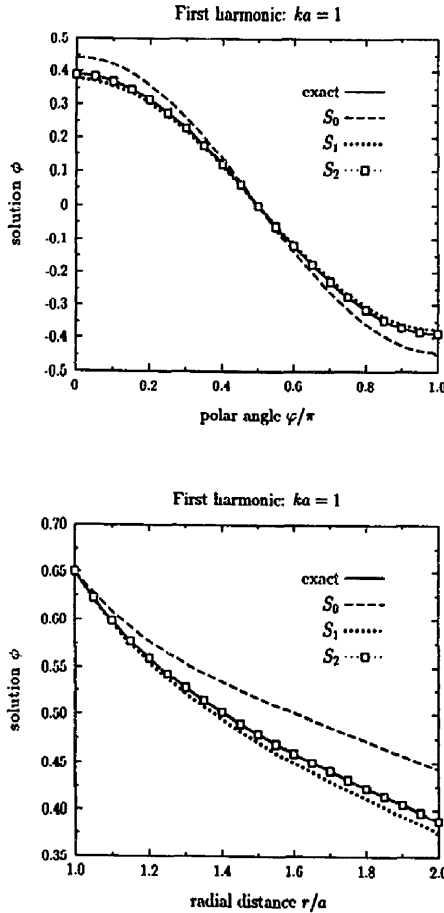


Fig. 4. Spherical wave harmonic $n = 1$. Results at $t = 20$, comparing the ‘plane-wave’ S_n , first-order S_1 and second-order S_2 boundary conditions. (Top): Solution profile on the artificial boundary $r = R$. (Bottom): Solution plotted along radial line at $\varphi = 0$.

somewhat out-of-phase with the exact steady-state solution while the simple ‘plane-wave’ damper S_0 , shows significant errors in both phase and amplitude. Contour plots illustrating the global character of the solution for $n = 1$ are given in Fig. 11.

To investigate the ability of the local non-reflecting boundary conditions to transmit higher-order spherical harmonics, the radiation loading in (70) was increased to $n = 2$. Fig. 5 shows a comparison of the space–time solution at time $t = 15$, using the local boundary operators S_j , $j = 0, 1, 2$. The numerical results using the low-order operators S_0 and S_1 show a significant error in the solution, while the solution using S_2 remains relatively accurate with only a small error in amplitude, see the time history in Fig. 9.

Numerical solutions for harmonic loading with $n = 3$, with a driving frequency of $ka = 1$ begin to deteriorate in accuracy for all three local boundary operators tested; although the solution using S_2 in comparison to the low-order operators still gave the most accurate solution. When the non-dimensional wavenumber is increased to $ka = 3$, i.e. by setting the driving frequency to $\omega = 1$ with a wave speed $c = 1/3$, the solution using S_2 is remarkably accurate; with the numerical and analytical solutions

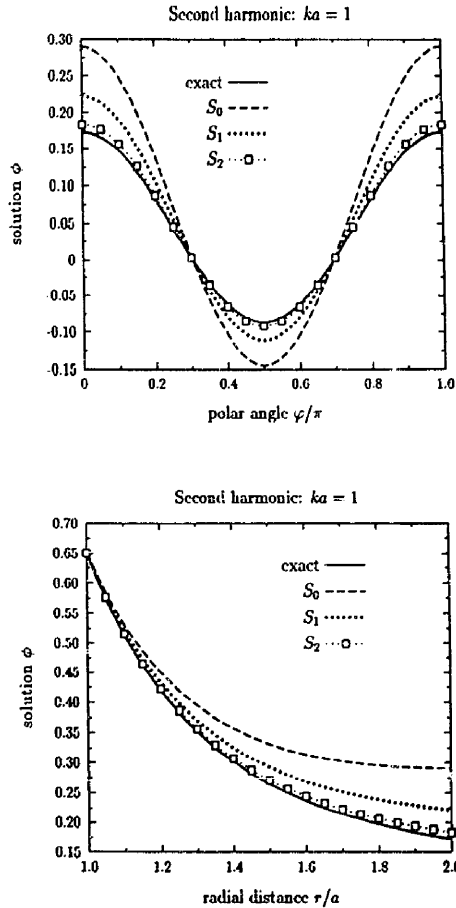


Fig. 5. Spherical wave harmonic $n = 2$. Results comparing the 'plane-wave' S_0 , first-order S_1 and second-order S_2 , boundary conditions. (Top): Solution profile on the artificial boundary $r = R$. (Bottom): Solution plotted along radial line at $\varphi = 0$.

almost indistinguishable, see Figs. 6, 10 and 12. Results using S_0 and S_1 for a frequency $ka = 3$ show significant errors in the solution, although less error than for $ka = 1$. This example demonstrates an important property of the approximate local boundary conditions: As the frequency, normalized with respect to the characteristic dimension of the problem increases, the accuracy of the local boundary conditions increases.

Figs. 7 and 10 (bottom) show the solution for the spherical harmonic $n = 4$ with a non-dimensional wavenumber $ka = 3$ at time $t = 15$. For this radiation loading, the S_2 local operator is still able to maintain an accurate solution, while the solution using the low-order operators S_0 and S_1 have deteriorated significantly. When the radiation loading is raised to harmonic $n = 5$, the accuracy of S_2 has finally begun to deteriorate as shown in Fig. 8. In this case, the solutions obtained using S_0 and S_1 display a dramatic loss of accuracy, indicating that their ability to transmit outgoing waves without reflection has been greatly diminished. In order to obtain accurate solutions for this harmonic and frequency, the boundary operator must be increased beyond second order, or the artificial boundary must be moved further away from the radiating sphere, requiring a larger computational domain, and a subsequent increase in computational expense.

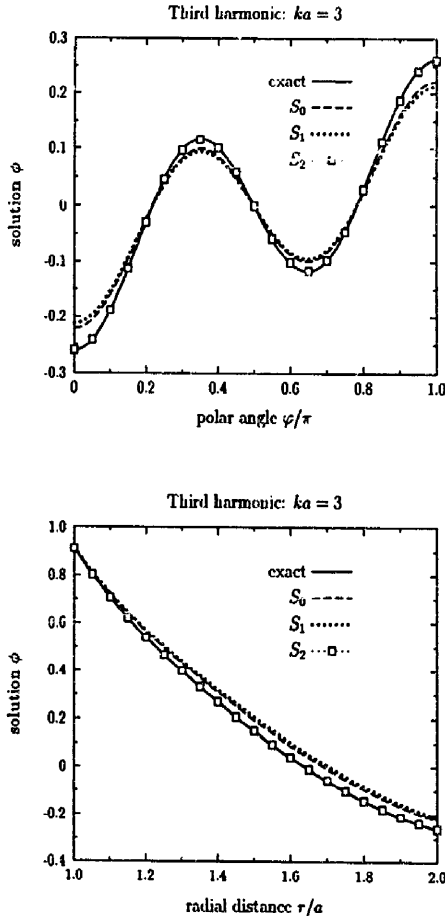


Fig. 6. Spherical wave harmonic $n = 3$. Results at $t = 20$, comparing the 'plane-wave' S_0 , first-order S_1 and second-order S_2 boundary conditions. (Top). Solution profile on the artificial boundary $r = R$. (Bottom): Solution plotted along radial line at $\varphi = 0$.

5.2. Non-concentric spherical radiator

In this example, the performance of the absorbing boundary conditions when implemented in the space-time formulation is evaluated for a transient radiation problem involving the propagation of a finite-duration pulse. Consider a sphere of radius $r = a$, pulsating with a uniform sine pulse, $\phi(a, t) = \sin \omega t$ and $\omega = \pi$, during the short time interval $t \in [0, 1]$. The transform of this time signal is characterized by an infinite band of frequencies centered about the dominant frequency of the excitation. Initial conditions are set to zero and the wave speed is $c = 1$. The exact solution to this problem is an outgoing spherical wave of short duration with a $1/r$ amplitude decay:

$$\phi(r, t) = \left(\frac{a}{r}\right) \sin \omega(t - \bar{r}/c) \tag{72}$$

where $\bar{r} = r - a$ is the radial distance from the spherical radiator and $(t - \bar{r}/c) \in [0, 1]$.

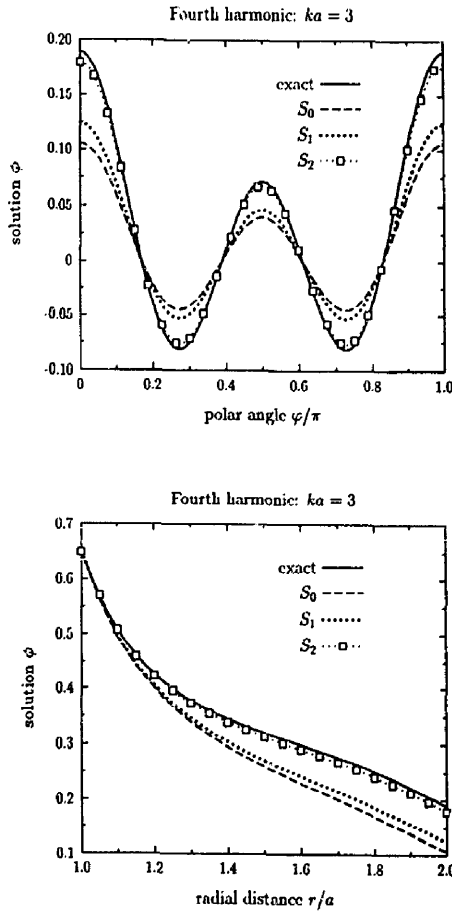


Fig. 7. Spherical wave harmonic $n = 4$. Results comparing the ‘plane-wave’ S_0 , first-order S_1 and second-order S_2 boundary conditions. (Top): Solution profile on the artificial boundary $r = R$. (Bottom): Solution plotted along radial line at $\varphi = 0$.

If the radiating sphere is placed concentric with a spherical artificial boundary, as was done in the previous example, then for the radiation field given in (72), the problem is trivial in that the first-order S_1 , and our higher-order local non-reflecting boundary conditions are all exact by design. In order to obtain a challenging problem, the radiating sphere is shifted from the center of the spherical artificial boundary Γ_x , to a non-concentric position. In this example, the radiating sphere is offset by a distance a , with the radius of Γ_x set at $R = 3a$, see Fig. 13. With this positioning, wave fronts traveling outward along radial lines will strike the artificial boundary at oblique angles. The closer the radiating sphere gets to the edge of Γ_x , the more acute this angle becomes, making it increasingly difficult for the approximate local boundary conditions to transmit outgoing waves without spurious reflection.

Fig. 14 shows the computational domain discretized with 1518 axisymmetric elements using quadratic interpolation. Fig. 15 shows the elevated contours of the time-discontinuous Galerkin solution using the second-order local boundary operator S_2 applied to Γ_x . In the upper left corner of Fig. 15, the solution

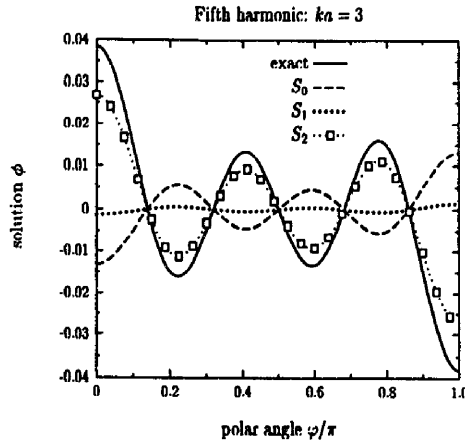


Fig. 8. Spherical wave harmonic $n=5$. Results comparing the 'plane-wave' S_0 , first-order S_1 and second-order S_2 boundary conditions. Solution profile on the artificial boundary $r=R$.

is shown at the end of the initial sine pulse at time $t=1$. As time progresses, the initial pulse propagates outward from the sphere as a uniform spherical wave pulse of decreasing amplitude. The scales used in the illustrations are normalized at each time step to enhance the visibility of the solution features. After $t=1$, the spherical pulse begins to pass through the artificial boundary Γ_x with negligible reflection. These results illustrate the remarkable performance of our second-order operator S_2 to transmit waves striking the artificial boundary at rather severe angles. At time $t=3.5$, as the pulse is just leaving the computational domain, it is noted that the numerical solution displays insignificant traces of low amplitude reflected waves behind the outgoing wave front. These low amplitude reflected waves are barely visible in the figure and their amplitude is several orders of magnitude smaller than the amplitude of the physical wave, indicating an accurate solution. For time steps beyond $t=4$ (not shown), the small amplitude residual waves are quickly damped out by the numerical dissipation inherent in the time-discontinuous Galerkin method.

For comparison, this same problem was solved with the low-order boundary operator S_1 . Fig. 16 shows a snapshot of the elevated contours at time $t=2.5$, comparing the solution using either S_1 or S_2 . Results for S_1 exhibit significant reflections as the outgoing pulse passes through Γ_x , as indicated by the elevated contours on the right-hand side of the sphere. In comparison, the solution using S_2 shows no observable reflections from Γ_x . This conclusion is summarized in Fig. 17 with a time-history of the solution on the artificial boundary Γ_x at the axis of symmetry, $\varphi=0$. The solution using S_2 shows the correct amplitude and phase for the outgoing pulse and shows no observable reflections behind the wave front. In contrast, the solution using S_1 shows an increase in the maximum amplitude of the outgoing pulse as well as significant reflections, as manifested by the non-zero amplitudes appearing for times $t>2$.

5.3. Radiation from a circular piston on a sphere

To study a problem involving an infinite number of spherical wave harmonics, consider the radiation from a circular piston subtending a polar angle $0 \leq \varphi \leq \varphi_p = 13.5^\circ$ on a submerged sphere of radius

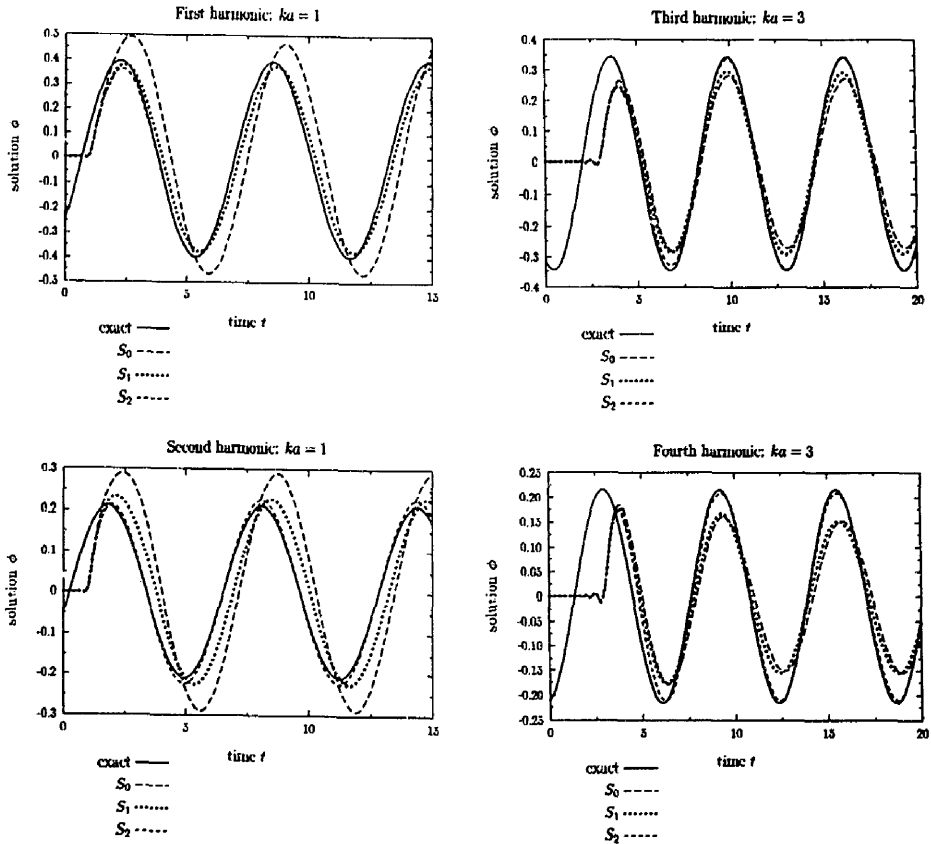


Fig. 9. Time-dependent solution at a point on the artificial boundary, i.e. $r = R$ and $\varphi = 0$. Results show the transient solution as it is driven to steady-state for (top) $n = 1$, and (bottom) $n = 2$.

Fig. 10. Time-dependent solution at a point on the artificial boundary, i.e. $r = R$ and $\varphi = 0$. Results show the transient solution as it is driven to steady-state for (top) $n = 3$, and (bottom) $n = 4$.

$r = a$; see Fig. 18. The piston has a constant inhomogeneous value $\phi(a, t) = \sin \omega t$ for $t > 0$. Elsewhere on the wet surface, the solution vanishes. The steady-state analytical solution for the velocity potential is

$$\phi(r, \varphi, t) = -\frac{1}{2} \text{Imag} \left\{ \sum_{n=0}^{\infty} \frac{h_n(kr)}{h_n(ka)} [P_{n-1}(\cos \varphi_p) - P_{n+1}(\cos \varphi_p)] P_n(\cos \varphi) e^{-i\omega t} \right\} \quad (73)$$

This problem gives rise to the interesting feature that as the wave generated at the piston pole $\varphi = 0^\circ$, travels along longitudes, it is attenuated by a geometrical spreading loss. As the diameter of the sphere increases when compared to a wavelength, the wave field departs more and more from a point source pattern, and in the region opposite the piston pole $\varphi = 180^\circ$, the amplitude is significantly lower.

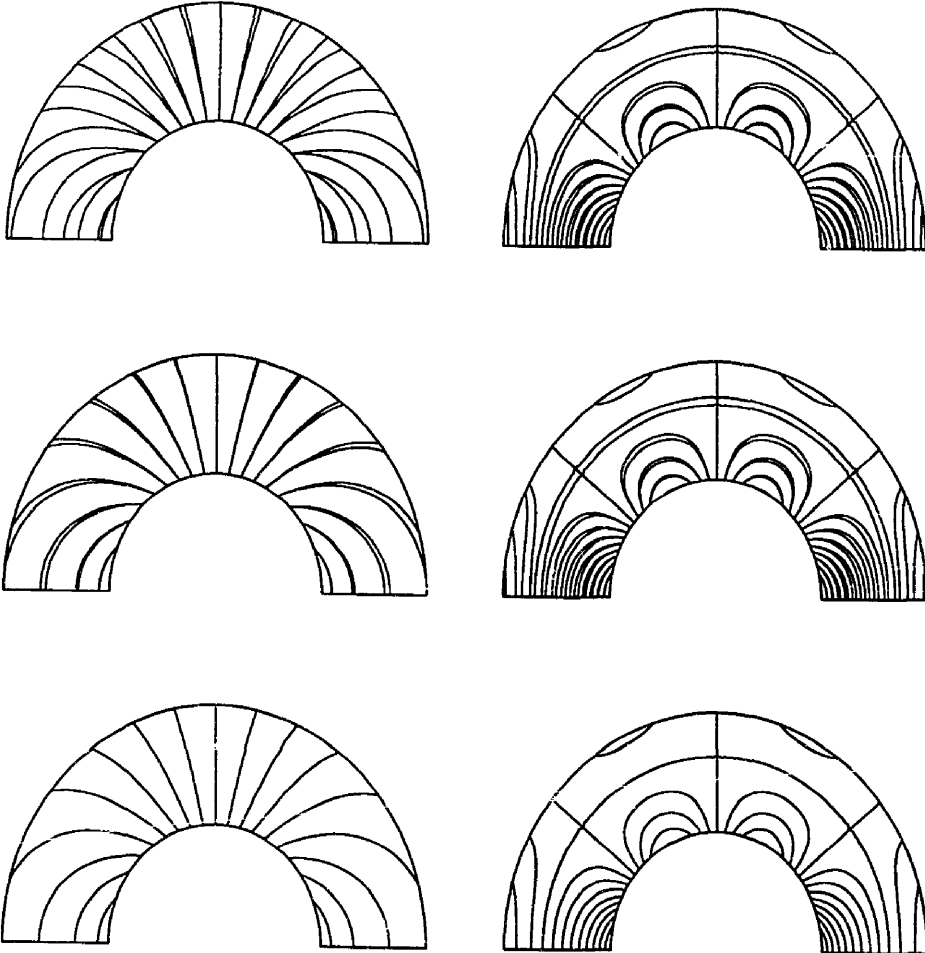


Fig. 11. Radiation from a sphere with polar harmonic $n = 1$ and normalized frequency $ka = 1$. Contours of space-time solution at $t = 20$ using local boundary conditions, (Top): 'plane-wave' \mathcal{S}_0 , (Middle): first-order \mathcal{S}_1 , (Bottom): second-order \mathcal{S}_2 . Dotted contours denote analytical solution. Scale: (Max 0.650, Min -0.650).

Fig. 12. Radiation from sphere with polar harmonic $n = 3$ and normalized frequency $ka = 3$. Contours of space-time solution at $t = 20$ using local boundary conditions, (Top): 'plane-wave' \mathcal{S}_0 , (Middle): first-order \mathcal{S}_1 , (Bottom): second-order \mathcal{S}_2 . Dotted contours denote analytical solution. Scale: (Max 0.913, Min -0.913).

In this example, the properties and discretization are unchanged from the spherical harmonic radiation problem in the first example. Fig. 19 (top) shows the contours of the analytical series solution, nodally interpolated with the mesh employed. The low-amplitude oscillations in the vicinity of the wet surface are a product of the difficulty the series solution has in resolving the discontinuity in the loading condition at $\varphi_p = 13.5^\circ$, and are not relevant to the validation of the numerical results. The steady-state solution obtained by the time-discontinuous solution is shown in Fig. 19 (middle) and (bottom), for the \mathcal{S}_1 and \mathcal{S}_2 operators, respectively. Results for the space-time solution show a significant improvement

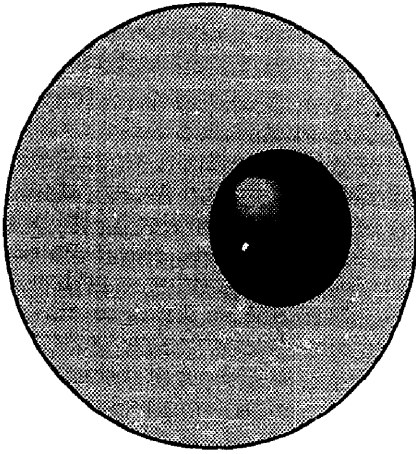


Fig. 13. Illustration of a spherical radiator of radius a , offset from the center of a spherical artificial boundary of radius $3a$.

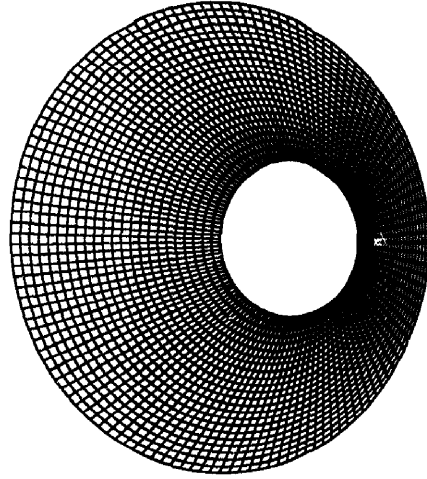


Fig. 14. Computational domain for a sphere shifted from the center of a spherical non-reflecting boundary. Spatial discretization: Upper half modeled with 1518 axisymmetric elements using quadratic interpolation.

in the solution using \mathcal{S}_2 , in comparison to the solution using \mathcal{S}_1 . Near the piston pole, both solutions accurately capture the physics of the problem, but as the wave pattern spreads to the backside, the solution using \mathcal{S}_1 deteriorates significantly while \mathcal{S}_2 maintains an accurate solution throughout the entire computational domain.

5.4. Illustration of stability

In this example we illustrate the need for the temporal jump terms on the absorbing boundary Γ_x . Fig. 20 shows the time history at a point on Γ_x for the transient radiation from a circular cylinder that is driven to steady-state. The solid line in Fig. 20 is the exact time-harmonic solution for this problem. For this two-dimensional problem, we use the sequence of high-order approximate local boundary conditions described in [18, 19], which are based on the radial asymptotic solution to the wave equation in two dimensions. In particular, the following second-order local time-dependent boundary operator is used for this problem.

$$\mathcal{S}_2\phi = \frac{1}{2R} \left(3/4 - \frac{\partial^2}{\partial\theta^2} \right) \phi + \frac{3}{2c} \dot{\phi} + \frac{R}{c} \frac{\partial\phi}{\partial r} + \frac{R}{c^2} \ddot{\phi} \quad (74)$$

Details for the implementation of this two-dimensional boundary operator in the time-discontinuous finite element method are given in [14]. Results from this example demonstrate that when the consistent jump terms defined in (57) are included on the boundary Γ_x , then the solution using the local boundary condition \mathcal{S}_2 displays the correct transient solution for short time (time less than 6 s), and then quickly assumes the exact steady-state solution. However, when the temporal jump terms are omitted, i.e.

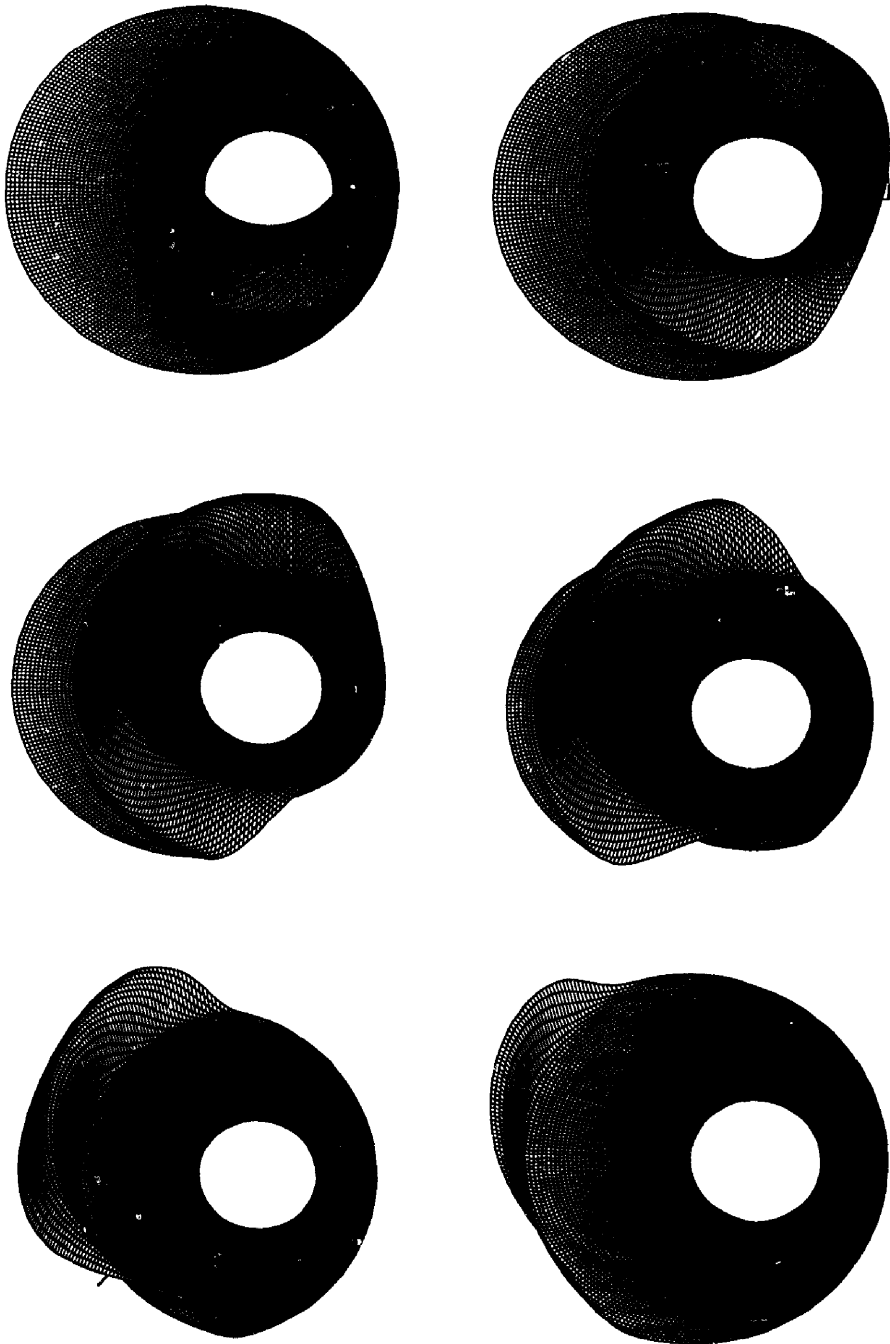


Fig. 15. Radiation from a non-concentric sphere. Elevated solution contours shown at the end of the initial pulse at $t=1$ and later times $t=1.5$ through $t=3.5$ in increments of $\Delta t=0.5$.

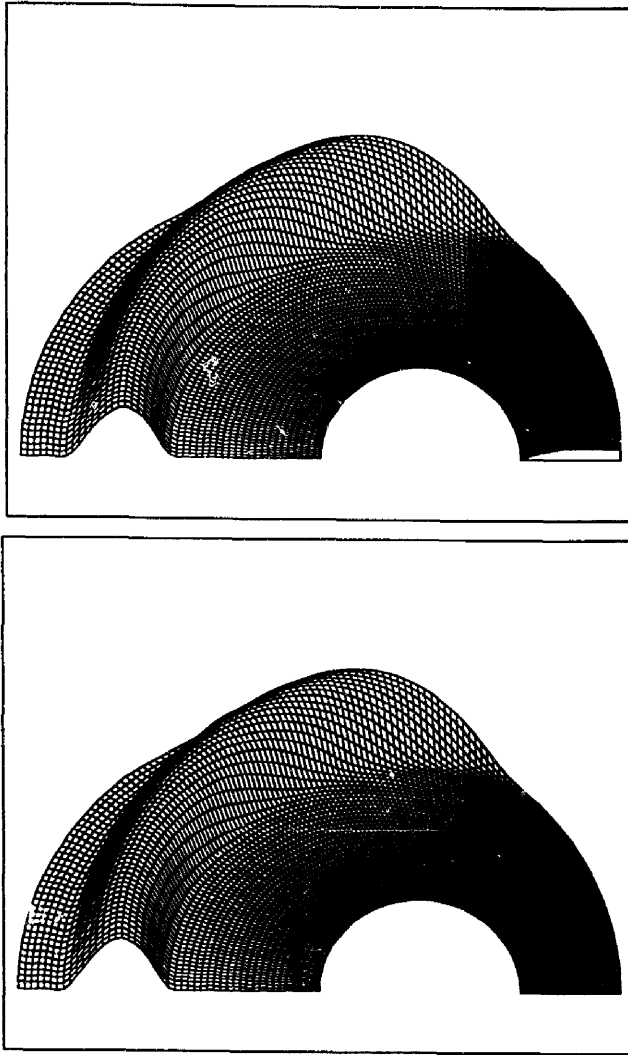


Fig. 16. Radiation from a non-concentric sphere. Elevated contours shown at $t = 2.5$. Space-time solution using (top) \mathbb{S}_1 local boundary condition. (bottom) \mathbb{S}_2 local boundary condition.

$$d_2(w^h(t_n^+), \llbracket \phi^h(t_n) \rrbracket)_{\Gamma_c} = 0$$

$$d_0(w^h(t_n^+), \llbracket \phi^h(t_n) \rrbracket)_{\Gamma_c} = 0$$

then the solution quickly becomes unstable, generating large spurious oscillations, eventually leading to overflow. This example demonstrates how these additional operators are needed to ensure a stable solution, and are the key element that enable generalization of the time discontinuous Galerkin method to handle non-reflecting boundary conditions.

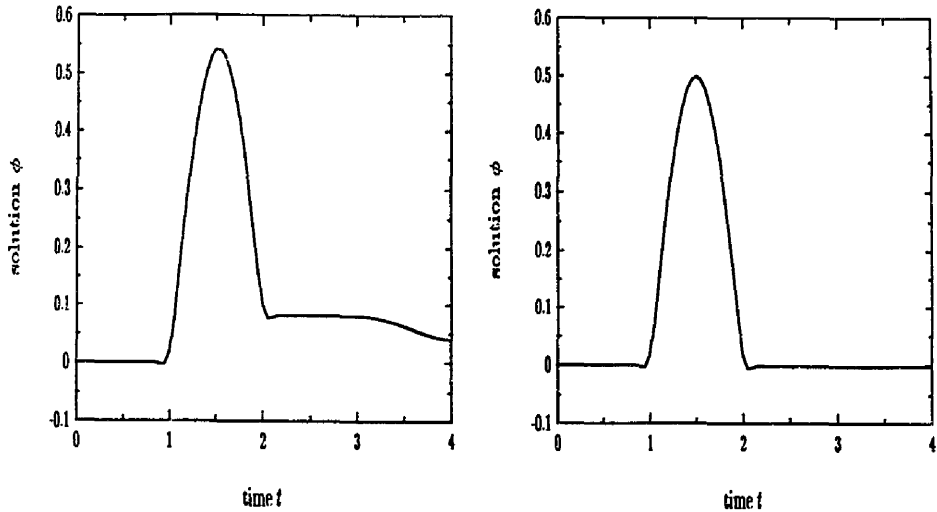


Fig. 17. Radiation from a non-concentric sphere: Solution on the artificial boundary Γ_a , at the axis of symmetry $\varphi = 0$. (left) S_1 local boundary condition. (right) S_2 local boundary condition.

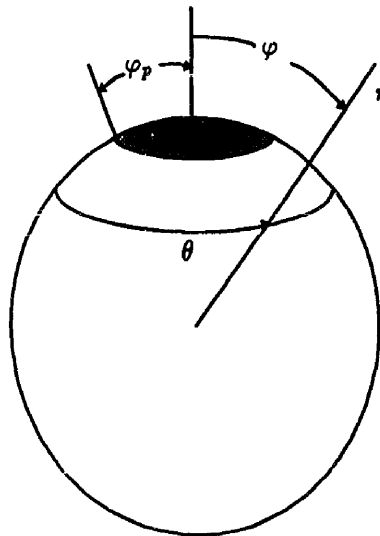


Fig. 18. Illustration of a circular piston subtending a polar angle φ_p in a spherical baffle of radius a .

6. Conclusions

In Part 1 [7], a new space-time finite element method for structural acoustics was given. The formulation employs a finite computational fluid domain surrounding the structure and incorporates local time-dependent non-reflecting boundary conditions on the fluid truncation boundary. Non-

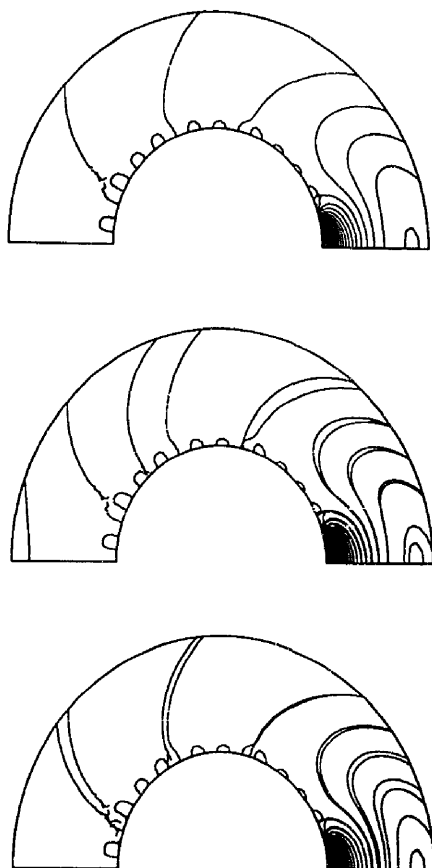


Fig. 19. Solution contours for radiating piston on a sphere. (Top): Analytic series solution at time $t = 30$ and $ka = 3$. (Middle): Space-time solution with \mathcal{S}_1 . (Bottom): Space-time solution with \mathcal{S}_2 . Dotted contours denote exact solution. Scale: (Max 0.048, Min -0.988).

reflecting boundary conditions are incorporated as ‘natural’ boundary conditions in the space-time variational equation, i.e. they are enforced weakly in both space and time.

In this paper, new local time-dependent non-reflecting boundary conditions which are exact for the first N spherical wave harmonics have been developed for the scalar wave equation in three space dimensions. The development of these boundary conditions began with the truncated Dirichlet-to-Neumann (DtN) map in the frequency domain. Time-dependent boundary conditions that are local in both time and space were obtained by an inverse Fourier transform. The time-discontinuous Galerkin space-time formulation provides a natural variational setting for the incorporation of these local in time boundary conditions, where standard C^0 continuous interpolations in the time dimension may be used up to the order required by the boundary operator. Crucial to the stability and convergence of our time-discontinuous Galerkin method for structural acoustics in infinite domains is the introduction of consistent temporal jump operators across space-time slabs restricted to the radiation boundary. The specific form of these operators were designed such that continuity of the solution across slabs is weakly enforced in a form consistent with the exact non-reflecting boundary conditions. However, for boundary conditions beyond second-order, high-order continuity in the space dimension on the

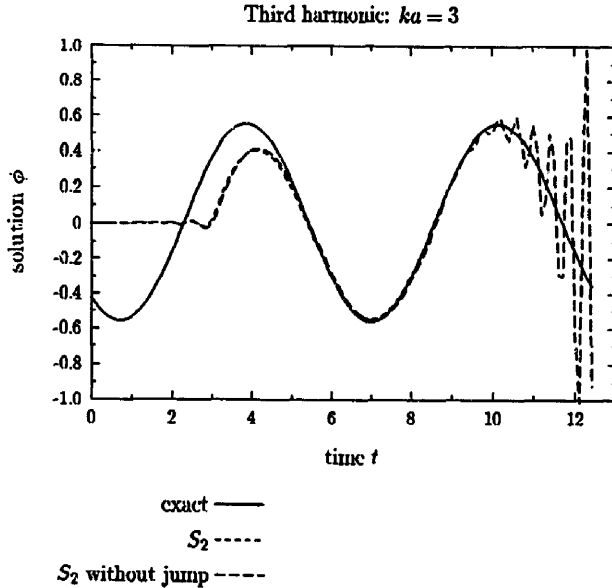


Fig. 20. Illustration of stability. Radiating circular cylinder with loading $\cos 3\theta \sin \omega t$. Results at the artificial boundary Γ_x demonstrate that temporal jump terms are needed on Γ_x for stability.

boundary is required due to the high-order tangential derivatives appearing in the operators. To address this issue, we derived an exact local in time counterpart for the spatially non-local and frequency dependent DtN non-reflecting boundary condition. This resulted in a new sequence of exact boundary conditions that retain their locality in time yet require a non-local spatial integral. The advantage of these new local in time and non-local in space non-reflecting boundary conditions is that they allow for the use of C^0 interpolations in both the time and space dimensions.

Because the time-dependent boundary conditions were derived from the exact impedance for the exterior fluid outside the artificial boundary Γ_x , and do not depend on the form of governing equations within the interior computational region Ω , they are applicable to both radiation and scattering from rigid or elastic structures, and for any number of inhomogeneities or non-linearities within the bounded computational domain.

A feature inherited by the non-reflecting boundary conditions proposed in this paper is that they exactly represent the solution as a series of outgoing spherical wave harmonics. This property plays an important role in the understanding of how individual wave harmonics contribute to the accuracy and stability of the solution as effected by the radial distance of the artificial boundary from the source, the geometric complexity of the wave pattern and the frequency content of the outgoing waves. In contrast, a physical understanding of the harmonic contribution to the accuracy and stability of boundary operators based on approximate power series (multipole) expansions, such as the popular Bayliss and Turkel sequence of boundary operators is lacking.

Numerical solutions for some representative transient acoustic radiation problems demonstrated the improved accuracy and efficiency that results from the use of the high-order non-reflecting boundary conditions within our space-time finite element formulation. In particular, the effects of increasing spherical harmonics n , frequency $\omega = kc$, and the position of the truncation boundary R , on the accuracy of the space-time finite element solution using the new local non-reflecting boundary operators was investigated. Results from this study are summarized in the following:

- (1) The local boundary operators provide increasing accuracy with the order N used in the truncated DtN series, allowing for the use of smaller fluid meshes with a subsequent gain in efficiency.

- (2) When the solution on the artificial boundary consists of only the first N wave harmonics, then the boundary conditions are exact in both time and space.
- (3) The accuracy for higher wave harmonics depends strongly on the normalized frequency ka , in that the local operators can accurately capture increased wave harmonics as the frequency (wavenumber) is increased relative to the dimension of the radiator/scatterer.
- (4) The operators are increasingly accurate for higher wave harmonics as the position R of the artificial boundary is moved further away from the radiator/scatterer.

Results from these studies, together with the numerical results obtained from a vibrating piston on a spherical baffle, and the transient radiation from a non-concentric sphere, support the conclusion that the second-order absorbing boundary condition S_2 , when implemented in the time-discontinuous Galerkin formulation, exhibits superior accuracy (for the same position) when compared to the low-order plane-wave damper S_0 or spherical damper S_1 , resulting in a drastic reduction in the computational domain needed, with a corresponding reduction in computational cost and storage. Additional numerical examples are reported in [6, 8]. These results suggest that the new high-order non-reflecting boundary conditions provide an economical means to achieve accurate solutions to the transient structural acoustics problem in infinite domains.

While the numerical implementation presented in this paper have been limited to boundary conditions up to second order, the time-discontinuous space-time finite element formulation is applicable to third and higher-order boundary conditions; research efforts are under way to address the implementational issues of the high-order boundary conditions. Third and higher-order boundary conditions involve fourth and higher-order time derivatives, which can be implemented efficiently by employing space-time elements with fourth and higher-order temporal interpolation on the face adjacent to the radiation boundary Γ_x and low-order temporal interpolation on the other faces. It remains to be seen what (if any) additional advantage in terms of accuracy and economy can be achieved by the implementation of the high-order operators beyond second order. The implementation and numerical analysis of local time-dependent absorbing boundary conditions in two spatial dimensions are reported in [8, 14].

In the numerical examples given in this paper, a very regular mesh was used. A refinement/unrefinement strategy for transient structural acoustics that truly adapts to the character of the solution simultaneously in both time and space dimensions would lower the solution costs significantly. A successful adaptive scheme would track the propagation of waves as they propagate along space-time characteristics. The space-time finite element approach advocated in this work provides a powerful framework for unified and simultaneous spatial and temporal adaptivity of the discretization. We are actively pursuing the development of efficient and accurate local error indicators to drive the implementation of adaptive strategies for the space-time finite element solution of the exterior structural acoustics problem incorporating our exact time-dependent non-reflecting boundary conditions.

Acknowledgments

This research was sponsored by the Office of Naval Research under Contract Numbers N00014-89-J-1951 and N00014-92-J-1774. The first author was also partially supported by an Achievement Rewards for College Scientists (ARCS) fellowship. We would also like to thank Greg Hulbert for access to the source code of his modified version of the computer program DLEARN.

References

- [1] R.D. Mindlin and H.H. Bleich, Response of an elastic cylindrical shell to a transverse, step shock wave, *J. Appl. Mech.* 20 (1953) 189–195.
- [2] J.B. Keller and D. Givoli, Exact non-reflecting boundary conditions, *J. Comp. Phys.* 82 (1989) 172–192.
- [3] D. Givoli, A spatially exact non-reflecting boundary condition for time-dependent problems, *Comput. Methods Appl. Mech. Engrg.* 95 (1992) 97–113.

- [4] D. Givoli and J.B. Keller, Non-reflecting boundary conditions for elastic waves, *Wave Motion* 12 (1990) 261–279.
- [5] I. Harari, Computational methods for problems of acoustics with particular reference to exterior domains, Ph.D. Dissertation, Stanford University, Stanford, CA, 1991.
- [6] L.L. Thompson and P.M. Pinsky, New space-time finite element methods for fluid–structure interaction in exterior domains, in: *Computational Methods for Fluid/Structure Interaction*, AMD-Vol. 178 (ASME, 1993) 101–120.
- [7] L.L. Thompson and P.M. Pinsky, A space–time finite element method for structural acoustics in infinite domains, Part 1: Formulation, stability and convergence. *Comput. Methods Appl. Mech. Engrg.* 132 (1996) 195–227.
- [8] L.L. Thompson, Design and analysis of space–time and Galerkin/least-squares finite element methods for fluid–structure interaction in exterior domains, Ph.D. Dissertation, April 1994, Stanford University, Stanford, CA, 1994.
- [9] B. Engquist and A. Majda, Absorbing boundary conditions for the numerical simulation of waves, *Math. Comput.* 31 (1977) 629–652.
- [10] B. Engquist and A. Majda, Radiation boundary conditions for acoustic and elastic calculations, *Comm. Pure Appl. Math.* 32 (1979) 313–357.
- [11] A. Bayliss and E. Turkel, Radiation boundary conditions for wave-like equations, *Comm. Pure Appl. Math.* 33 (1980) 707–725.
- [12] A. Bayliss, M. Gunzburger and E. Turkel, Boundary conditions for the numerical solution of elliptic equations in exterior regions, *SIAM J. Appl. Math.* 42 (1982) 430–451.
- [13] K.F. Graff, *Wave Motion in Elastic Solids* (Dover, New York, 1975).
- [14] L.L. Thompson and P.M. Pinsky, A space–time finite element method for the exterior structural acoustics problem: Time-dependent radiation boundary conditions in two space dimensions, *Int. J. Numer. Methods Engrg.*, in press.
- [15] L.F. Kallivokas, J. Bielak and R.C. MacCamy, Symmetric local absorbing boundaries in time and space, *ASCE J. Engrg. Mech.* 117(9) (1991) 2027–2048.
- [16] G.M. Hulbert, Space–time finite element methods for second-order hyperbolic equations, Ph.D. Dissertations, Stanford University, Stanford, CA, 1989.
- [17] G.M. Hulbert and T.J.R. Hughes, Space–time finite element methods for second-order hyperbolic equations, *Comput. Methods Appl. Mech. Engrg.* 84 (1990) 327–348.
- [18] P.M. Pinsky and L.L. Thompson, Accuracy of local non-reflecting boundary conditions for time-dependent structural acoustics, NCA-Vol. 12/AMD-Vol. 128, *Structural Acoustics* (ASME, 1991) 153–160.
- [19] P.M. Pinsky, L.L. Thompson and N.N. Abboud, Local high-order radiation boundary conditions for the two-dimensional time-dependent structural acoustics problem, *J. Acoust. Soc. Am.* 91(3) (1992) 1320–1335.